Journal of
Mechanics of
Materials and Structures

AN AXISYMMETRIC PARACHUTE MODEL WITH WRINKLING

Yoav Ofir, Dan Givoli and Avinoam Libai

Volume 6, No. 1-4 January–June 2011

mathematical sciences publishers

JOURNAL OF MECHANICS OF MATERIALS AND STRUCTURES
Vol. 6, No. 1-4, 2011

msp

AN AXISYMMETRIC PARACHUTE MODEL WITH WRINKLING

YOAV OFIR, DAN GIVOLI AND AVINOAM LIBAI

We are honored to dedicate this paper to Charles Steele and to the memory of Marie-Louise Steele.
Charles was my admired teacher at Stanford, and has opened my eyes to the wonderful world of shells.
Marie-Louise was a friend who always had a few warm words for a PhD student undergoing stressful times.
I will always remember her very fondly. – Dan Givoli

The deformation and stresses in a parachute canopy are analyzed, using an axisymmetric model. The canopy is modeled as an ideal or nearly ideal elastic membrane shell. Steady state is assumed. No restriction is imposed on the size of the deformation, and thus the problem is strongly nonlinear. Wrinkles which form over parts of the surface are taken into consideration approximately via the use of wrinkle fields (tension fields). The solution is obtained by a double-iteration numerical procedure, based on a shooting technique and incremental loading. First a basic parachute model is considered in which the material is assumed isotropic and Hookean, the pressure distribution is assumed uniform (but with unknown magnitude), and the canopy is assumed to have a small central hole. Later all these assumptions are relaxed. Numerical examples are presented for some representative cases.

1. Introduction

Analysis of deformation and stresses in a parachute under general conditions is extremely complicated. Treatment of the full problem in the literature is scarce; the impressive computational work of Tezduyar's group [Stein et al. 2000; 2001] and that of [Kim and Peskin 2006; 2009], which takes into account the complete fluid-structure interaction, should be mentioned in this context. The structural analysis of the canopy is considered, for example, in [Liu et al. 2001; Lu et al. 2001]. These two papers take into account the *wrinkles* which are generally formed in the parachute canopy. Information on such wrinkles is important since they may affect the deformation and stress distribution in the canopy and thus may have an influence on the overall parachute performance.

In this paper we propose a much simpler method of analysis for parachutes. Although the actual behavior of real parachutes and their design are beyond the scope of this paper, we briefly mention a few facts related to this subject, with particular attention to the issues of shape, stability, and wrinkles. The classical paper [Taylor 1919] recognized that "if stability were the chief thing to be desired, a parachute in the form of rounded cone is desirable... If lightness is the most important quality, it appears that one should make one's parachute as flat as possible, provided it will remain distended. If, however, the parachute is made too flat, radial crinkles or pleats will appear and these must mean a waste of material." Taylor then proceeds to determine the optimal deformed shape of a parachute, and obtains a theoretical shape determined by elliptic function curves. He comments that this theoretical shape differs from actual shapes of parachutes in that the curvature of the profile near the edge is smaller in the former, and he attributes this to the assumption of uniform pressure underlying his analysis.

Keywords: axisymmetric membrane shell, tension field, wrinkle field, parachute, canopy.

The parachute studied in [Taylor 1919] assumes that inextensible wires woven into the fabric extend radially from the center to the edge. In between these wires the fabric bulges out, to form a lobed shape. In contrast, the parachute considered in the present paper is assumed to be *axisymmetric*, and therefore cannot account for canopy lobes. Admittedly, axisymmetry is rather a strong simplification in practical parachute analysis, since it neglects the presence of the lobes. Moreover, in some cases the axisymmetric solution may be an *unstable* equilibrium solution of the parachute problem, while a stable solution deviates from the axisymmetric configuration. Baginski et al. [2006] and Deng and Pellegrino [2008] demonstrate such symmetry-breaking clefting in the case of pumpkin balloons. In the case of smooth surfaces, wrinkles coalesce and form a small number of localized folds, as in Mylar party balloons. Both papers obtain stable solutions that deviate from the axisymmetric shape as the pressure is decreased from a nominal value by using detailed three-dimensional finite element analyses. The method of analysis proposed here is, of course, oblivious to all these effects, which is its main limitation. Despite this fact, we believe that the types of results that this simple method can produce are very helpful in preliminary design stages, and can serve as basis for more detailed asymmetric analysis.

In this context, the spectrum of analysis methods for parachutes should be recognized. On one end of this spectrum one can find the complete numerical analysis methods mentioned above, usually based on finite element discretization in space. On the other end of the spectrum are crude calculations or analytical solutions, usually associated with linear elasticity, namely with the assumption of small deformation and linear material behavior. Our proposed method is somewhere inside this interval; it does make a few basic assumptions, the most limiting of which being axisymmetry, but on the other hand it assumes neither small deformation nor linear material behavior.

The canopy may be thought of as an ideal or nearly ideal elastic membrane shell. Ideal membranes will wrinkle rather than support compressive stresses. Often this results in the formation of wrinkle zones over portions of the deformed surface. These zones, in which the principal stress resultants are everywhere nonnegative, provide a mechanism for carrying the imposed loads. Within a wrinkle zone, the crests and troughs of the wrinkles are parallel to the direction of principal tension, and the stress resultant in the direction normal to them (in the tangent plane) vanishes.

The parachute behaves essentially as a pulled axisymmetric membrane with surface of positive Gaussian curvature. To illustrate the basic phenomena involved, Figure 1 describes the behavior of a model of a membrane with surface of positive Gaussian curvature, albeit significantly simpler than that of the

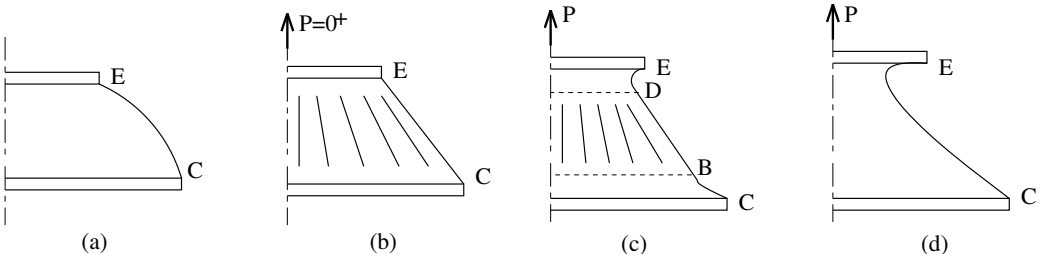

Figure 1. Wrinkles forming in an axisymmetric pulled membrane: (a) the unloaded membrane; (b) the wrinkled cone generated by a slight pulling force; (c) the wrinkle region (BD) and the two doubly tense regions (CB and ED) formed by a medium-sized pulling force; (d) the all-tense surface generated by a large pulling force.

parachute to be discussed later. The membrane is subjected to a pulling force, as was considered in [Libai and Givoli 2002]. The membrane is attached to two rigid plates along its two edges C and E, as shown in Figure 1a. The bottom plate is assumed to be fixed, whereas the top plate is pulled upwards. During the pull, the upper plate remains parallel to the lower plate and does not rotate with respect to it. The application of a slight pulling force $P = 0^+$ to the upper plate results in the formation of meridional wrinkles, and the membrane surface becomes a "wrinkled cone;" see Figure 1b. The formation of wrinkles is due to the fact that the circumferential stress resultants, which would have existed in such a membrane, must be negative, and are replaced by the wrinkle field. In addition, the requirements of equilibrium in the direction of the normal to the membrane demand that the curvature of the meridional lines be zero. Thus, the meridional wrinkle field takes on the shape of a cone.

In the vast majority of materials for membranes, a Poisson-like effect exists, such that a tensile stress in one direction is accompanied by contraction (negative strain) in the directions normal to it. If this contraction were prevented, say, along a boundary, then positive stresses would form along it and in its immediate neighborhood. The rigid plates at the upper and lower edges of the membrane prevent the transverse contraction, which would have occurred due to the pulling, and, thus, positive circumferential stresses accompany the positive pulling stresses. A biaxial state of stress is, thus, formed at and near the edges. The size of the edge zones is $o(e)$, where e is a typical meridional strain; see [Libai 1990]. The entire effect is strongly nonlinear.

An increase in the pulling force leads to a corresponding increase in e, so that the edge zones deteriorate. Thus, increasingly larger doubly tense regions are formed near the boundaries, where both the meridional and tangential (hoop) stress resultants are positive, while the central region remains wrinkled, as illustrated in Figure 1c. In the absence of internal pressure, the meridional curvature of the surface in the doubly tense regions is always negative; see, for example, [Libai and Simmonds 1998; Libai and Givoli 2002]. A further increase in the force causes the central wrinkle region to shrink, until, finally, a tensile *biaxial* state of stress exists over the entire surface; see Figure 1d.

In the case of large wrinkle zones in a membrane, direct and full treatment of the wrinkles is generally difficult. This fact gave rise to the notion of *wrinkle fields*, or *tension fields*, which represent the wrinkles in a "homogenized" sense. The basic idea in the theory of wrinkle fields is to avoid studying the wrinkle region in detail by replacing it with a smoothed-out *pseudosurface*. This pseudosurface must be in equilibrium, and the minimum principal stress resultant must vanish on it. Obviously, the stretch of the pseudosurface in the direction of the zero minimum principal stress resultant is nonphysical, in that it is not equal to that of the actual wrinkled surface.

In [Wu 1978] the first complete treatment of wrinkling in nonlinearly elastic membranes of revolution was given. Zak [1982] extended the theory to wrinkling of films of arbitrary shape. Pipkin [1986] proposed the notion of "relaxed energy density" in this context. Steigman and coworkers have made extensive theoretical studies [Steigmann and Pipkin 1989; Steigmann 1990; Li and Steigmann 1995a; 1995b] of the behavior of wrinkled and partly wrinkled membranes in various cases, including that of pressurized spherical and toroidal membranes. Libai [1990] presented a complete theoretical analysis of the transition zone between the doubly tense and wrinkle regions for pulled spherical membranes. Tait et al. [1996] and Tait and Connor [1997] solved wrinkling problems for cylindrical membranes. Roddeman et al. [1987a; 1987b], Jeong and Kwak [1992], Chiu et al. [1993], and Muttin [1996] developed finite element methods for the solution of partly wrinkled membranes. See [Libai and Simmonds 1998,

Chapters 5 and 7] for a detailed exposition on the subject and additional references. Recent publications making computational use of wrinkle fields for various applications include [Raible et al. 2005; Cavicchi et al. 2009; Mosler and Cirak 2009; Liu and Sze 2009].

In this paper we use wrinkle fields to analyze the deformation and stresses in a parachute canopy, using an axisymmetric model. We model the parachute as an ideal or nearly ideal elastic membrane shell. "Nearly ideal" means that the membrane is allowed to sustain small compressive stresses; it wrinkles only under larger compressive stresses. Thus, the minimal principal stress resultant is N_{cr}, where N_{cr} is a nonpositive parameter assumed to be a material property. For ideal membranes $N_{\mathrm{cr}} = 0$, and for nearly ideal membranes N_{cr} has a small negative (given) value.

The idea to use $N_{\mathrm{cr}} \neq 0$ in a membrane was suggested in [Rimrott and Cvercko 1986] in the context of pulled flat rectangular membranes. The authors claim that the formation of a *finite* number of wrinkles, which is typically observed in experiments in real membranes, is evidence of the presence of some small bending stiffness, since in the absence of such stiffness there should be an infinite number of wrinkles. Based on the experimental observation that, after the initial wrinkles form, additional deformation does not affect their number, Rimrott and Cvercko obtained a relation which connects the parameter N_{cr} to the number of wrinkles in the membrane, that is, to the wavelength of a single wrinkle. This relation can be exploited to effectively measure N_{cr} by counting the number of wrinkles.

Wong and Pellegrino [2006] derive another relation, based on a simple buckling model, in which N_{cr} depends on the material properties (Young's modulus and Poisson's ratio), the thickness of the membrane, and the half-wavelength of the wrinkle. They use this relation and the condition $N_\theta = N_{\mathrm{cr}}$ (where N_θ is the transverse stress resultant) to calculate the wrinkle half-wavelength, namely the number of wrinkles.

In the present paper we calculate solutions for both ideal membranes ($N_{\mathrm{cr}} = 0$) and nearly ideal membranes ($N_{\mathrm{cr}} < 0$). In the latter case, our choice for the value of N_{cr} is rather arbitrary and does not necessarily correspond to an actual membrane material and thickness. We simply increase $|N_{\mathrm{cr}}|$ from zero until the effect of this parameter becomes significant. Choosing N_{cr} in a more judicious way would require an additional analysis, such as that of Wong and Pellegrino.

We assume steady state, namely that the canopy is fully open and the air pressure acting on it is quasistatic. On the other hand, we pose no restriction on the size of the deformation, which may be very large, thus making the problem strongly nonlinear. We solve the problem using a double-iteration numerical procedure, based on a shooting technique and incremental loading. We demonstrate that the method works very well despite the complexity of the problem which involves the highly nonlinear membrane shell equations, different regions with interfaces which are unknown a priori, and deformation-dependent pressure magnitude.

We first consider a basic parachute model in which we assume the material to be isotropic and Hookean, the pressure distribution to be uniform, although with an unknown magnitude, and the canopy to have a small hole in its center. Later we relax all these assumptions and consider also an orthotropic canopy (which allows us to represent the higher stiffness in the meridional direction due to the canopy cords), neo-Hookean material, nonuniform pressure (with a known distribution but unknown magnitude), and canopies without a central hole. In the latter case, some numerical difficulties arise near the apex, and we overcome them by slightly modifying the calculation procedure in the apex vicinity.

Summary. In Section 2 we present the parachute model and its governing equations. In Section 3 we outline the computational scheme for the solution of the parachute problem, for the basic model. In

Section 4 we discuss the four extensions mentioned above. In Section 5 we present some representative numerical results. We end with some concluding remarks in Section 6.

2. Parachute model and governing equations

2.1. ***Basic model and notation.*** We consider a thin curved axisymmetric hyperelastic membrane with a positive Gaussian curvature (the canopy) subjected to a given axial pulling force P (the carried weight), as illustrated in Figure 2. The meridian of the membrane extends between points C and E. The force P is transferred to the canopy through tensed cords of given length L, which must be tangential to the meridian at point C (see Figure 2) since the membrane has no bending stiffness. The entire model is axisymmetric, and thus the cords are represented by a continuous "cone" revolving around the axis of symmetry. The tension of this "axisymmetric cord" in the deformed configuration is denoted T, and the angle it forms with the axial direction β, both unknown. The pressure acting on the membrane is assumed to be uniform, but its magnitude, denoted p, is unknown.

The upper edge of the shell, point E, is fixed to a rigid ring of given radius, which encloses and reinforces a small hole in the center of the canopy. For arbitrary external forces P and p, an axial reaction force R would act at this point. Since the parachute is known to be in equilibrium under P and p alone, we require that this reaction vanish, that is, $R = 0$, which will give us a condition that will be essential in determining the pressure p.

We expect the membrane to have doubly tense regions near the lower and upper edges, and possibly a wrinkle field in a central region of the meridian, bounded by points B and D (see Figure 2).

We define the notation needed to describe the geometry of the shell. The surface of the unloaded membrane is described by the function $r = r(z)$, where r and z are the radial and axial coordinates,

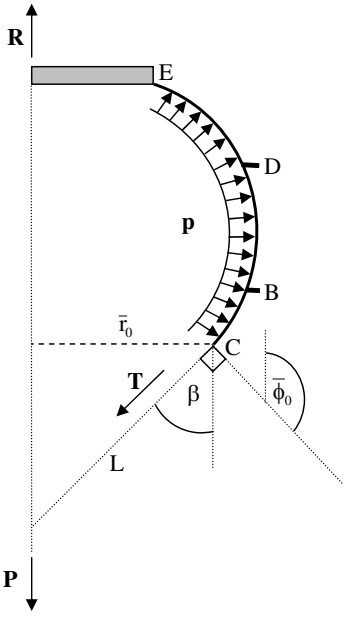

Figure 2. The basic parachute model.

respectively. The arc length coordinate along the meridian is denoted s. We use a superposed bar to denote quantities in the deformed configuration. Thus, we let $\bar{r}$, $\bar{z}$, and $\bar{s}$ denote, respectively, the radial, axial, and arc length locations of a material point in the deformed configuration. Thus, the surface of the deformed membrane is described by the function $\bar{r} = \bar{r}(\bar{z})$. We let $\bar{\phi}$ be the angle between the axial direction and the normal to the deformed surface. We denote quantities related to the lower edge of the meridian (point C) by the subscript 0. Thus, $\bar{\phi}_0$ is the angle $\bar{\phi}$ at the lower edge in the deformed configuration.

We let N_s and N_θ be the meridional and tangential stress resultants per unit undeformed length, and $\bar{N}_s$ and $\bar{N}_\theta$ be the meridional and tangential stress resultants per unit deformed length. We let λ_s and λ_θ be the principal stretches.

2.2. ***Governing equations and boundary conditions.*** In this section we summarize all the equations and boundary conditions that constitute our model. We first write down all the equations that hold in a doubly tense region, and then we comment on the changes that need to be made in these equations in a wrinkle region.

Basic relations connecting quantities in the deformed and undeformed configurations. Classical relations of axisymmetric membrane shell theory are used. The relations among the stress resultants are given by

$$r N_s = \bar{r}\bar{N}_s, \qquad ds N_\theta = d\bar{s}\bar{N}_\theta, \tag{1}$$

which actually *define* the stress resultants in the undeformed configuration. The principal stretches are related to the geometry through

$$\lambda_s = d\bar{s}/ds, \tag{2}$$

$$\lambda_\theta = \bar{r}/r. \tag{3}$$

Axial equilibrium. Consideration of the axial equilibrium of a portion of the membrane which lies on the lower side of a circumferential cross section yields

$$P - 2\pi\bar{r}\bar{N}_s \sin\bar{\phi} - I = 0, \tag{4}$$

where

$$I \equiv \int_0^{\bar{s}} 2\pi p \bar{r}' \cos\bar{\phi}' \, d\bar{s}'. \tag{5}$$

The integral I is the total axial force due to the pressure p acting from the lower edge of the membrane along the meridian up to the point under consideration. A prime ($'$) denotes a quantity calculated at the integral variable point $\bar{s}' \in [0, \bar{s}]$. Using (1) in (4) we also obtain

$$N_s = \frac{P - I}{2\pi r \sin\bar{\phi}}. \tag{6}$$

This equation holds in the entire membrane.

Normal equilibrium. In the doubly tense regions, we also consider the normal equilibrium of an element, which yields the equation

$$\frac{\bar{N}_\theta}{\bar{\rho}_\theta} + \frac{\bar{N}_s}{\bar{\rho}_s} = p. \tag{7}$$

Here, $\bar{\rho}_s$ and $\bar{\rho}_\theta$ are the meridional and tangential radii of curvature of the deformed membrane, which satisfy

$$\frac{1}{\bar{\rho}_s} = -\bar{\phi}_{,\bar{s}}, \qquad \bar{\rho}_\theta = \frac{\bar{r}}{\sin\bar{\phi}}. \tag{8}$$

In (8) and elsewhere, a comma indicates differentiation. We use (1), (7), and (8) to obtain

$$N_\theta = \frac{rN_s\bar{\phi}_{,s} + p\bar{r}\bar{s}_{,s}}{\sin\bar{\phi}}. \tag{9}$$

Substituting N_s from (6) yields

$$N_\theta = \frac{p\bar{r}\bar{s}_{,s}}{\sin\bar{\phi}} - \frac{(\cot\bar{\phi})_{,s}}{2\pi}(P - I). \tag{10}$$

Compatibility equation. The *compatibility relation* simply relates $\bar{r}$, $\bar{s}$, and $\bar{\phi}$ through

$$\frac{d\bar{r}}{d\bar{s}} = -\cos\bar{\phi}. \tag{11}$$

The minus sign in (11) comes from the fact that in the region where the cosine is positive, namely where $\bar{\phi} < \pi/2$ (for example, as in the segment CB shown in Figure 1c), $\bar{r}$ is a decreasing function of $\bar{s}$.

Constitutive relations. The constitutive relations complete the set of differential equations governing the membrane's behavior. It is assumed that the membrane is isotropic hyperelastic, namely it possesses a strain energy function $W(\lambda_s, \lambda_\theta)$ per unit area of the undeformed surface, such that

$$N_s = W_{,\lambda_s}, \qquad N_\theta = W_{,\lambda_\theta}, \tag{12}$$

in the doubly tense regions.

In our basic model we consider a *Hookean* (linear elastic) isotropic material. In this case, the strain energy function is quadratic:

$$W(\lambda_s, \lambda_\theta) = \frac{Eh}{1-\nu^2}\left(\tfrac{1}{2}(\lambda_s^2 + \lambda_\theta^2) + \nu\lambda_s\lambda_\theta - (1+\nu)(\lambda_s + \lambda_\theta - 1)\right). \tag{13}$$

Here h is the membrane thickness, E is the Young's modulus and ν is the Poisson's ratio. With this strain energy function, the relations (12) in the doubly tense regions become

$$N_s = \frac{Eh}{1-\nu^2}(\lambda_s + \nu\lambda_\theta) - \frac{Eh}{1-\nu}, \tag{14}$$

$$N_\theta = \frac{Eh}{1-\nu^2}(\lambda_\theta + \nu\lambda_s) - \frac{Eh}{1-\nu}. \tag{15}$$

Modified equations in the wrinkle region. Equations (1), (2), (4)–(6), and (11) hold in the entire membrane. The other equations written above hold in the doubly tense regions, and have to be modified in the wrinkle region. Equation (3) is not relevant in the wrinkle region since λ_θ is not physical there. Equation (10) is simply replaced by $N_\theta = N_{\rm cr}$ in the wrinkle region. Here $N_{\rm cr}$ is a nonpositive quantity assumed to be a material property. For ideal membranes $N_{\rm cr} = 0$, and for nearly ideal membranes $N_{\rm cr}$ has a small negative (given) value.

The constitutive equations (14) and (15) are replaced by an effective constitutive equation in the wrinkle region. Since $N_\theta = N_{\rm cr}$ there, (15) furnishes then a relation between λ_s and λ_θ. This relation

can be used to eliminate λ_θ from (14), thus obtaining a modified unidirectional constitutive relation for N_s. After some algebra, the end result is

$$N_s = Eh(\lambda_s - 1) + \nu N_{\mathrm{cr}}. \tag{16}$$

Geometrical relations at the lower edge. A few geometrical relations may be inferred from the setup shown in Figure 2, in the deformed configuration:

$$\bar{\phi}_0 = \beta + \pi/2, \tag{17}$$

$$\bar{r}_0 = L \sin\beta, \tag{18}$$

$$P = 2\pi \bar{r}_0 T \cos\beta. \tag{19}$$

From the last two relations, a simple relation between the unknown quantities β and T can be deduced:

$$T = \frac{P}{\pi L \sin 2\beta}. \tag{20}$$

Boundary and interface conditions. To complete the statement of the problem, the equations given above must be accompanied by boundary conditions at the two ends of the membrane. At the lower end (point C in Figure 2) we have

$$(\bar{N}_s)_0 = T, \tag{21}$$

since T is tangent to the meridian at this point. At the upper end (point E in Figure 2) we have

$$r_E = \bar{r}_E \quad \text{or} \quad (\lambda_\theta)_E = 1, \tag{22}$$

since the membrane is fixed to a rigid ring there. The second equality in (22) follows from (3).

We also need interface conditions at the meridional junctions of the doubly tense and wrinkle regions (points B and D in Figure 2). These conditions are:

$$N_\theta = N_{\mathrm{cr}} \quad \text{and} \quad \bar{\phi} \text{ is continuous} \qquad \text{at B and D.} \tag{23}$$

From (6) and (16) we conclude that N_s and λ_s are also continuous at the interfaces. This completes the statement of the problem for given pressure p.

Global equilibrium. Since the entire parachute is in self equilibrium under load P and pressure p, we must have

$$P - I_E = 0, \tag{24}$$

where I_E is the value of I defined by (5) at point E, which is the total axial force due to the pressure p along the entire meridian. This equation will serve us in determining the pressure p.

We remark that from (24) and (6) it follows that at point E either $N_s = 0$ or $\bar{\phi} = 0$. However, we do not enforce this boundary condition directly, but rather enforce the global equilibrium condition (24), as will be explained in the next section.

3. Computational scheme

3.1. ***The overall scheme.*** The problem involves a single *given* loading parameter, namely the carried weight P. We approach the parachute problem via *incremental loading*, by increasing the load P in small discrete steps from zero to its final value. This serves two purposes. First, for a given undeformed geometry of the canopy, this provides us with a family of solutions for various carried weights. Second, this procedure helps us to detect critical values of P for which essential changes occur in the nature of the solution.

For a given value of P, the computational scheme that we use in order to solve the problem stated in the previous section involves two nested iteration processes. The outer iteration loop may be described as follows. We make an initial guess $\tilde{p}$ for the pressure value p. Then we step into the inner iteration loop (to be described in the next subsection) and compute all deformation and stress variables along the entire meridian. Based on this solution, we calculate the reaction R (see Figure 2) by

$$R = P - I_E. \tag{25}$$

Of course, we know that R should vanish, since the whole parachute is self-equilibrated; see (24). Computationally, we check if the criterion

$$|R| \le \delta_1 P \tag{26}$$

is satisfied, where δ_1 is a small given tolerance. If this criterion is satisfied, our guess was correct, and thus $\tilde{p} \simeq p$ and the whole problem is solved. If not, we change the guess $\tilde{p}$ and repeat the inner iteration loop. This process continues, until (26) is satisfied.

Despite the strong nonlinear nature of the whole problem, numerical experiments show that the relation between the reaction R and the assumed applied pressure $\tilde{p}$ is almost linear! This is demonstrated in Figure 3, where the reaction-pressure relation is shown for a typical set of input parameters (ideal membrane, elliptic initial shape, vertical force $P = 0.1$). This surprising fact can be explained by the following calculation. Let us evaluate the integral I defined by (5) at the upper point E (see Figure 2) for a guessed pressure value $\tilde{p}$:

$$I_E = 2\pi\,\tilde{p} \int_0^{\bar{s}_E} \bar{r}' \cos\bar{\phi}'\, d\bar{s}'. \tag{27}$$

Defining

$$\hat{I}_E = \int_0^{\bar{s}_E} \bar{r}' \cos\bar{\phi}'\, d\bar{s}', \tag{28}$$

and using (25), we have

$$R(\tilde{p}) = P - 2\pi\,\tilde{p}\,\hat{I}_E. \tag{29}$$

We calculate $\hat{I}_E$ using (28), (3), (11), and (22):

$$\hat{I}_E = \int_0^{\bar{s}_E} \bar{r}' \cos\bar{\phi}'\, d\bar{s}' = -\int_{\bar{r}_0}^{\bar{r}_E} \bar{r}'\, d\bar{r}' = -\tfrac{1}{2}(\bar{r}_E^2 - \bar{r}_0^2) = -\tfrac{1}{2}(r_E^2 - \bar{r}_0^2) = -\tfrac{1}{2}\big(r_E^2 - r_0^2(\lambda_\theta)_0^2\big). \tag{30}$$

Now we make the assumption that the hoop strain at the lower point is small, namely that $(\lambda_\theta)_0$ is close to one. (This assumption was verified numerically in the example problems that we have solved.) We

write this assumption is the form

$$(\lambda_\theta)_0 = 1 + \epsilon f(\tilde{p}) = 1 + O(\epsilon). \tag{31}$$

Then from the last calculation we have

$$\hat{I}_E = -\tfrac{1}{2}\left(r_E^2 - r_0^2 + O(\epsilon)\right). \tag{32}$$

Using this result in (29) finally yields

$$R(\tilde{p}) = P + \pi\left(r_E^2 - r_0^2 + O(\epsilon)\right)\tilde{p}. \tag{33}$$

This is an approximate linear relation between R and $\tilde{p}$, which explains the observation above.

The fact that R is almost proportional with $\tilde{p}$ is a considerable aid in the numerical convergence of the scheme. By taking advantage of this fact, one is able to find an excellent approximation for the pressure p by making only two calculations, with two values of $\tilde{p}$, and linearly extrapolating the results as implied by Figure 3.

Incidentally, from the calculation above we can deduce another almost linear relation, namely the relation between the true pressure p and the weight P. With the true pressure we should get $R = 0$, and from (29) we thus have

$$P - 2\pi p \hat{I}_E = 0. \tag{34}$$

Therefore,

$$p = \frac{P}{2\pi \hat{I}_E}, \tag{35}$$

and using (32) we have

$$p = -\frac{P}{\pi(r_E^2 - r_0^2 + O(\epsilon))}. \tag{36}$$

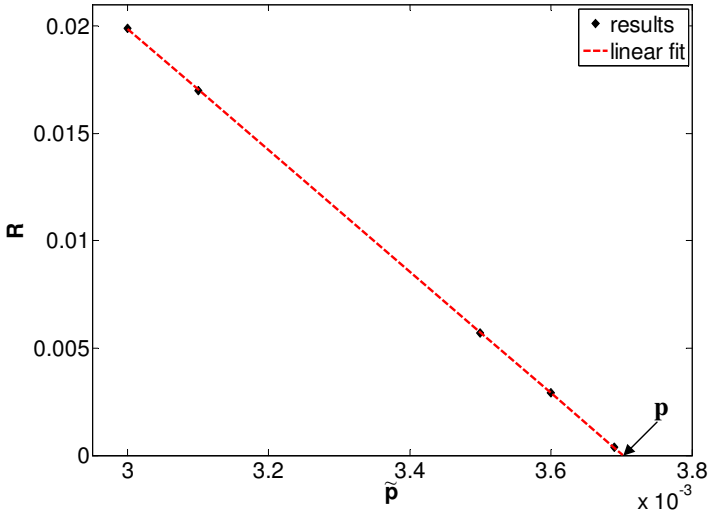

Figure 3. The reaction R as a function of the pressure $\tilde{p}$ for a typical set of input parameters. The five dots along the straight line correspond to the numerical results of five runs of the inner iteration loop with different values of $\tilde{p}$.

This proves the claim, which was also verified numerically. If the term $O(\epsilon)$ is dropped as an approximation, we get the simple result $p = P/[\pi(r_0^2 - r_E^2)]$ which can be obtained directly from summation of forces in the z direction, and is valid also in the case of no hole ($r_E = 0$).

3.2. ***The inner-loop iterative procedure.*** The inner-loop iteration procedure is a generalization of the one used in [Libai and Givoli 2002] to analyze a pulled membrane without internal pressure and with simpler boundary conditions. This procedure is based on a shooting technique and on approximately integrating the equations along the meridian. (The use of such a technique was suggested to the third author by D. J. Steigmann; see also [Li and Steigmann 1995a; 1995b]).

The numerical scheme is outlined as follows. The value of the pulling force P is given. Also given is the function $r(z)$ describing the shape of the unloaded membrane, where z ranges from 0 to the height of the undeformed membrane Z. We divide the z axis into M small intervals $[z_{m-1}, z_m]$ for $m = 0, \ldots, M$. For simplicity we take the intervals to be of uniform size $\Delta z \equiv z_m - z_{m-1} = Z/M$. We start from the lower edge of the membrane, that is, point C in Figure 2. To initiate the integration process, we first guess the value of the hoop stretch at point C, $(\lambda_\theta)_0$. Then we integrate the equations numerically as will be described shortly, until we reach the other edge, that is, point E. We check if the boundary condition (22) is satisfied at point E to within a desired precision; if it is, the solution process has terminated. If not, the guessed value of $(\lambda_\theta)_0$ is adjusted, and the integration starts all over again from point C. This process is repeated until the boundary condition (22) is satisfied at point E.

The scheme is now described in full detail. The value of a variable v at location z_m is denoted v_m. The pressure $\tilde{p}$ is assumed to be known, having been set in the outer loop.

(1) **The lower doubly tense zone (from point C to point B; see Figure 2).**

(a) Choose an initial value $(\lambda_\theta)_0$ for the hoop stretch at point C.

(b) Set $m = 0$, $s_0 = \bar{s}_0 = 0$, $z_0 = \bar{z}_0 = 0$ and I_0=0.

(c) Use (3), (17), (18), and (20) to compute

$$\bar{r}_0 = r_0(\lambda_\theta)_0, \quad \beta = \sin^{-1}(\bar{r}_0/L), \quad \bar{\phi}_0 = \beta + \pi/2, \quad T = P/(\pi L \sin 2\beta).$$

(d) Use the equilibrium equation (6) to calculate

$$(N_s)_m = (P - I_m)/(2\pi r_m \sin\bar{\phi}_m).$$

(e) Use the constitutive equation (14) to calculate $(\lambda_s)_m$ from $(N_s)_m$ and $(\lambda_\theta)_m$:

$$(\lambda_s)_m = \frac{1-\nu^2}{Eh}(N_s)_m - \nu(\lambda_\theta)_m + 1 + \nu.$$

(f) Use the constitutive equation (15) to calculate $(N_\theta)_m$ from $(\lambda_s)_m$ and $(\lambda_\theta)_m$.

(g) Check if $(N_\theta)_m \le N_{\mathrm{cr}}$. If yes, point B is reached (see Figure 2); move to step 2.

(h) Calculate

$$z_{m+1} = z_m + \Delta z, \quad \Delta r_m = r_{m+1} - r_m, \quad \Delta s_m = \sqrt{(\Delta r_m)^2 + (\Delta z)^2}, \quad s_{m+1} = s_m + \Delta s_m.$$

(i) Use (2) to calculate

$$\Delta\bar{s}_m = \Delta s_m(\lambda_s)_m, \qquad \bar{s}_{m+1} = \bar{s}_m + \Delta\bar{s}_m.$$

(j) Integrate the equilibrium equation (10) to calculate

$$\bar{\phi}_{m+1} = \cot^{-1}\big[\cot\bar{\phi}_m - \big(2\pi/(P - I_m)\big)\big(\Delta s_m (N_\theta)_m - \tilde{p}\bar{r}_m \Delta\bar{s}_m/\sin\bar{\phi}_m\big)\big].$$

(k) Use the compatibility equation (11) to calculate

$$\Delta\bar{r}_m = -\Delta\bar{s}_m \cos\bar{\phi}_{m+1}, \qquad \bar{r}_{m+1} = \bar{r}_m + \Delta\bar{r}_m.$$

(l) Use (3) to calculate

$$(\lambda_\theta)_{m+1} = \bar{r}_{m+1}/r_{m+1}.$$

(m) Calculate

$$\Delta\bar{z}_m = \sqrt{(\Delta\bar{s}_m)^2 - (\Delta\bar{r}_m)^2}, \qquad \bar{z}_{m+1} = \bar{z}_m + \Delta\bar{z}_m.$$

(n) Use (5) to calculate

$$I_{m+1} = I_m + 2\pi\,\tilde{p}\cos(\bar{\phi}_m)\bar{r}_m \Delta\bar{s}_m.$$

(o) Set $m \leftarrow m + 1$ and return to substep (d).

(2) **The wrinkle zone (from point B to point D; see Figure 2).**

(a) Calculate

$$z_{m+1} = z_m + \Delta z, \qquad \Delta r_m = r_{m+1} - r_m, \qquad \Delta s_m = \sqrt{(\Delta r_m)^2 + (\Delta z)^2},$$
$$s_{m+1} = s_m + \Delta s_m, \qquad \Delta\bar{s}_m = \Delta s_m (\lambda_s)_m, \qquad \bar{s}_{m+1} = \bar{s}_m + \Delta\bar{s}_m.$$

(b) Set $(N_\theta)_{m+1} = N_{\rm cr}$.

(c) Integrate the equilibrium equation (10) to calculate

$$\bar{\phi}_{m+1} = \cot^{-1}\big[\cot\bar{\phi}_m - \big(2\pi/(P - I_m)\big)(\Delta s_m N_{\rm cr} - \tilde{p}\bar{r}_m \Delta\bar{s}_m/\sin\bar{\phi}_m)\big].$$

(d) Use the compatibility equation (11) to calculate

$$\Delta\bar{r}_m = -\Delta\bar{s}_m \cos\bar{\phi}_{m+1}, \qquad \bar{r}_{m+1} = \bar{r}_m + \Delta\bar{r}_m.$$

(e) Use (5) to calculate

$$I_{m+1} = I_m + 2\pi\,\tilde{p}\cos(\bar{\phi}_m)\bar{r}_m \Delta\bar{s}_m.$$

(f) Use the equilibrium equation (6) to calculate

$$(N_s)_{m+1} = (P - I_{m+1})/(2\pi r_{m+1}\sin\bar{\phi}_{m+1}).$$

(g) Use the constitutive equation (16) to calculate $(\lambda_s)_{m+1}$ from $(N_s)_{m+1}$:

$$(\lambda_s)_{m+1} = 1 + \big(1/(Eh)\big)\big((N_s)_{m+1} - \nu N_{\rm cr}\big).$$

(h) Calculate

$$\Delta\bar{z}_m = \sqrt{(\Delta\bar{s}_m)^2 - (\Delta\bar{r}_m)^2}, \qquad \bar{z}_{m+1} = \bar{z}_m + \Delta\bar{z}_m.$$

(i) Use (3) to calculate a nonphysical value of λ_θ:

$$(\lambda_\theta^{\rm NP})_{m+1} = \bar{r}_{m+1}/r_{m+1}.$$

(j) Use the constitutive equation (15) to calculate a nonphysical value of $(N_\theta)_{m+1}$, denoted by $(N_\theta^{\mathrm{NP}})_{m+1}$, from $(\lambda_s)_{m+1}$ and $(\lambda_\theta^{\mathrm{NP}})_{m+1}$.
(k) Check if $(N_\theta^{\mathrm{NP}})_{m+1} \geq N_{\mathrm{cr}}$. If yes — point D is reached (see Figure 2); skip to step 3.
(l) Set $m \leftarrow m+1$ and return to substep (a).

(3) **The upper doubly tense zone (from point D to point E; see Figure 2).**
(a) Repeat substeps (d)–(f) and (h)–(o) of step 1. Continue the integration process till the last step $m = M$, namely till $z_m = Z$.
(b) Based on the value $(\lambda_\theta)_M$ at point E, calculate $\mu = |1 - (\lambda_\theta)_M|$. Check if $\mu < \delta_2$, where δ_2 is a predetermined small tolerance. If yes, the solution process has ended. Otherwise, adjust the value of $(\lambda_\theta)_0$ (see step 1, substep (a)) and start the whole process again.

Numerical experiments show that the adjustment of the value of $(\lambda_\theta)_0$ is easy in practice. The "output" $(\lambda_\theta)_M$ turns out to be a monotonely increasing function of the "input" $(\lambda_\theta)_0$, so by using a bisection-type technique the correct value of $(\lambda_\theta)_0$ can be found after a few trials. Numerical experiments also show that the convergence of the results as the number of subintervals M increases is fast. Moreover, the entire calculation is explicit and therefore very efficient. For example, we have used $M = 10{,}000$ for the problems presented in Section 5, and the running time in each case on a personal workstation was a few seconds. Thus, despite the fact that the solution process involves two nested iteration schemes, it is extremely fast.

4. Extensions

In the basic model described above the material was assumed isotropic and Hookean, the pressure distribution was assumed uniform, and the canopy was assumed to have a small hole in its center. Now we show how each of these assumptions may be relaxed.

4.1. ***Orthotropic canopies.*** In real parachutes, the canopy is stiffened with a finite number of meridional cords. Classical analysis [Taylor 1919] assumes that these cords are inextensible and the membrane forms lobes between each pair of adjacent cords. In the framework of our basic axisymmetric assumption, we cannot handle individual cords. Instead, we assume that the cords cause a *global* stiffening effect in the meridional direction. Thus we consider an effective canopy material which is homogeneous but orthotropic. Thus, different material properties are associated with the meridional and the circumferential directions. Of course, the only change caused by this extension in our formulation is in the constitutive equations (14)–(16).

We denote the meridional and circumferential Young's moduli by E_s and E_θ, and the corresponding Poisson's ratios by ν_s and ν_θ. Then, in the doubly tense regions, (14) and (15) are replaced by

$$N_s = \frac{E_s h}{1-\nu_s\nu_\theta}(\lambda_s + \nu_s\lambda_\theta) - \frac{E_s h}{1-\nu_s\nu_\theta}(1+\nu_s), \tag{37}$$

$$N_\theta = \frac{E_\theta h}{1-\nu_s\nu_\theta}(\lambda_\theta + \nu_\theta\lambda_s) - \frac{E_\theta h}{1-\nu_s\nu_\theta}(1+\nu_\theta). \tag{38}$$

In the wrinkle region, in which $N_\theta = N_{\mathrm{cr}}$, we obtain, in a similar manner to the isotropic case,

$$N_s = E_s h(\lambda_s - 1) + (E_s/E_\theta)\nu_s N_{\mathrm{cr}}, \tag{39}$$

which replaces (16).

These modified equations imply obvious changes in the algorithm presented in the previous section.

4.2. ***Neo-Hookean material.*** In the case of a neo-Hookean material, the strain energy function (13) is replaced by

$$W(\lambda_s, \lambda_\theta) = Ch\big(\lambda_s^2 + \lambda_\theta^2 + (\lambda_s\lambda_\theta)^{-2} - 3\big), \tag{40}$$

where C is a material constant. In this case the relations (12) in the doubly tense regions become

$$N_s = 2Ch(\lambda_s - \lambda_s^{-3}\lambda_\theta^{-2}), \tag{41}$$

$$N_\theta = 2Ch(\lambda_\theta - \lambda_s^{-2}\lambda_\theta^{-3}), \tag{42}$$

and the modified constitutive law in the wrinkle region becomes

$$N_s = 2Ch(\lambda_s - \lambda_s^{-2}). \tag{43}$$

It should be noted that this relation is valid for an ideal membrane only.

An algorithmic complication arises from the fact that the numerical scheme presented above requires (see steps 1, substep (e) and 2, substep (g)) the inversion of the constitutive equations (41) and (43), so that in the doubly tense regions λ_s is expressed explicitly in terms of N_s and λ_θ, and in the wrinkle region λ_s is expressed as a function of N_s. In the Hookean case this inversion was trivial, but in the neo-Hookean case it involves the solution of a quartic equation and a cubic equation. Closed-form formulas for the solutions of these two equations were obtained in [Libai and Givoli 2002] — an exact formula for the cubic equation and a 4th-order asymptotic solution for the quartic solution; see more details in [Libai and Givoli 2002].

4.3. ***Nonuniform pressure.*** The assumption of uniform pressure distribution is typically a reasonable one; in many cases the pressure on the canopy is nearly uniform except in a thin boundary layer near the outer edge of the membrane and the edge of the central hole (if any), where the pressure drops rapidly to the atmospheric pressure. However, in some cases a more significant deviation from uniformity occurs, which the analyzer may want to take into account.

To demonstrate this capability, we use as an example the pressure distribution found via computational fluid dynamics in [Sahu et al. 1995], and adopted in [Shannon 2001, p. 117]. According to this result, the internal pressure on the canopy is almost uniform but the external pressure is nonuniform, leading to a nonuniform net pressure, that reaches a maximum around the center of the meridian. By using a piecewise cubic polynomial approximation we interpolate this pressure distribution. This is shown in Figure 4 as a function $f(\chi)$ defined over the unit interval $\chi \in [0, 1]$. The actual pressure $p(s)$ can then be expressed as a function of the undeformed arc length coordinate s by

$$p(s) = p_0 f(s/S). \tag{44}$$

Here p_0 is the pressure magnitude, which is unknown as in the uniform-pressure case, and S is the total arc length of the meridian in the undeformed configuration, which can easily be computed in advance from the known geometry of the undeformed meridian.

Obvious changes have to be applied to the algorithm presented in the previous section in order to replace the uniform pressure by the nonuniform pressure (44).

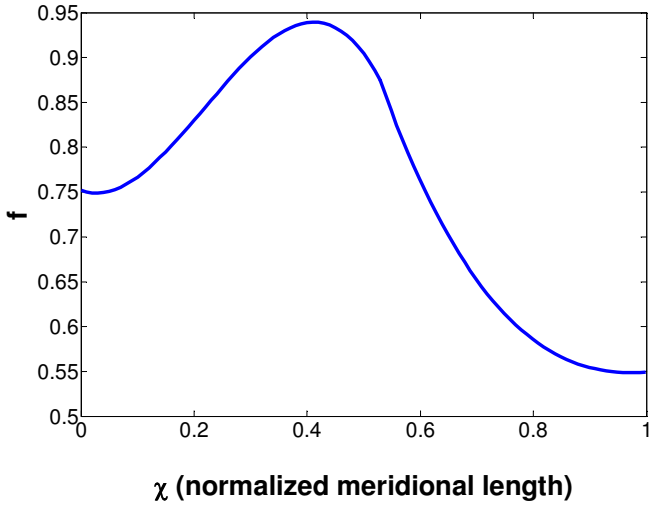

Figure 4. Nonuniform pressure distribution function, after [Sahu et al. 1995].

4.4. ***Canopy without a hole.*** The most involved extension to the basic setup presented in Section 2 is the consideration of a canopy without a central hole, as shown in Figure 5.

The governing equations in this case are identical to those in Section 2. However, the boundary condition (22) at point E needs to be modified. At the apex E we require that the membrane be continuous and have no kink (and thus must be flat there), namely

$$\bar{r}_E = 0, \qquad \bar{\phi}_E = 0. \tag{45}$$

From the condition $\bar{\phi}_E = 0$ and from (6), we deduce that (24) is also satisfied, and thus we do not need to require global equilibrium as an additional condition.

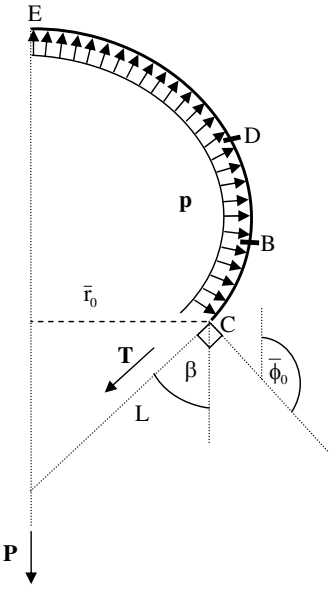

Figure 5. Parachute model with no hole.

A numerical difficulty arises when trying to apply the inner-loop scheme presented in Section 3.2 to this case. In the close vicinity of the apex, owing to the conditions $\bar{r}_E = 0$ and $\bar{\phi}_E = 0$, we have $\bar{r} \simeq 0$, $\bar{\phi} \simeq 0$, and $P - I \simeq 0$, and we also know that $r \simeq 0$. These approximate equalities give rise to large roundoff errors near the apex. For example, using $(\lambda_\theta)_{m+1} = \bar{r}_{m+1}/r_{m+1}$ (see the inner-loop scheme, step 1, substep (l), which is repeated in step 3) becomes impossible, since the quantity on the right side approaches a $0/0$ type limit at the apex.

To circumvent this difficulty, we approximate the deformed shape of the membrane in the close vicinity of the apex by the parabola

$$\bar{z}(\bar{r}) = a\bar{r}^2 + b\bar{r} + c, \tag{46}$$

where a, b, and c are constants. A similar technique has been used in the context of hot air balloon analysis [Irvine and Montauban 1980]. In that paper, the governing equations are simple enough to observe that in the limit $r \to 0$ an equation of a circle is obtained near the apex; therefore, for a 1° arc near the apex the shape of the membrane is assumed to be circular. In our case, the equations are not simple enough to observe the actual limit. However, in assuming the parabolic shape (46) we are guided by the fact that any smooth contour can be locally approximated by a parabolic curve.

We assume that (46) is the form of the deformed membrane when the condition $\bar{\phi} < \epsilon_\phi$ is satisfied, where ϵ_ϕ is a predetermined tolerance. This defines the point Q on the meridian, where the usual equations are to be replaced by modified equations based on the approximation (46). Since the parabola must be flat at the apex, we require

$$\frac{\partial \bar{z}}{\partial \bar{r}}\Big|_{\bar{r}=0} \equiv b = 0. \tag{47}$$

With the form (46) and (47) given, it is easy to calculate the limit of $\bar{r}/\bar{\phi}$ at the apex, and we find

$$\bar{r}/\bar{\phi} \simeq \bar{r}/\tan\bar{\phi} = \bar{r}/(-d\bar{z}/d\bar{r}) = -1/(2a). \tag{48}$$

Equations (47) and (48) are used in the scheme to pose two practical conditions on a and b:

$$|b| < \epsilon_1, \qquad 1/2 + (\bar{r}/\bar{\phi})a < \epsilon_2, \tag{49}$$

where ϵ_1 and ϵ_2 are given tolerances. We note that the second condition involves the ratio $\bar{r}/\bar{\phi}$ that is numerically problematic at the apex. However, this condition is checked only at point Q, which is on the *border* of the apex region where roundoff error is not yet significant.

In the close vicinity of the apex, the canopy behaves like a flat circular membrane under axisymmetric tension. Therefore we can assume

$$\lambda_s \simeq \lambda_\theta \simeq \text{constant}, \qquad N_s \simeq N_\theta \simeq \text{constant}. \tag{50}$$

From this and (3) we deduce

$$\lambda_s = \lambda_\theta = \frac{\bar{r}_Q}{r_Q}. \tag{51}$$

From axial equilibrium calculated from the apex to the point under consideration (see (4), which is calculated from the lower edge) we obtain, with $\eta = \bar{S} - \bar{s}$,

$$2\pi\bar{r}\bar{N}_s \sin\bar{\phi} = \int_0^{\bar{\eta}} 2\pi p\bar{r}' \cos\bar{\phi}'\, d\bar{\eta}'. \tag{52}$$

We use $\sin\bar{\phi} \simeq \bar{\phi}$, $\cos\bar{\phi} \simeq 1$, and $\bar{\eta} \simeq \bar{r}$, calculate the integral, and finally use (48) to get

$$\bar{N}_s \simeq -p/4a. \tag{53}$$

Using this result with (50), (1), and (3) we have

$$N_\theta = N_s = -\frac{p}{4a}\frac{\bar{r}_Q}{r_Q}. \tag{54}$$

Accordingly, step 3 in the inner-loop scheme of Section 3.2 should be modified for the case of no central hole in the following manner:

(3) **The upper doubly tense zone (from point D to point E; see Figure 2).**

(a) Repeat substeps (d)–(f) and (h)–(o) of step 1. Continue the integration process till the condition $\bar{\phi} < \epsilon_\phi$ is satisfied. Once this condition is satisfied, point Q is reached; denote the current meridional-step m by m_Q, and proceed to (b).

(b) Use the values of $\bar{r}$ and $\bar{z}$ at the last three grid points (m_Q, $m_Q - 1$, and $m_Q - 2$) to perform parabolic extrapolation and compute the constants a, b, and c in the parabola (46).

(c) Check the condition $1/2 + (\bar{r}_Q/\bar{\phi}_Q)a < \epsilon_2$ (see (49)). If it is satisfied, proceed to (d). Otherwise, adjust the value of $(\lambda_\theta)_0$ (see step 1, substep (a)) and start the whole process again.

(d) Calculate $\lambda_s = \lambda_\theta = \bar{r}_Q/r_Q$ and $N_\theta = N_s = -(p/4a)(\bar{r}_Q)(r_Q)$. These values are valid in the interval from Q to E.

(e) For $m = m_Q, \ldots, M$ calculate $\bar{r}_m = \lambda_\theta r_m$, $\bar{\phi}_m = -2a\bar{r}_m$, and $\bar{z}_m = a\bar{r}_m^2 + c$.

In the *outer loop* (see Section 3.1), we check if the condition $|b| < \epsilon_1$ (see (49)) is satisfied. If it is, our guess for $\tilde{p}$ was correct, and thus $\tilde{p} \simeq p$ and the whole problem is solved. If not, we change the guess $\tilde{p}$ and repeat the inner iteration loop. This process continues, until the condition $|b| < \epsilon_1$ is satisfied.

5. Numerical examples

We apply the proposed method to two example canopies, which differ in their initial (undeformed) shape. We consider a parabolic undeformed membrane described by

$$r(z) = -1.9z^2 + 2.9z + 2, \quad z \in [0, 2], \tag{55}$$

and an elliptic undeformed membrane described by

$$r(z) = 3.3\sqrt{1 - (z-1)^2/4}, \quad z \in [0, 2.99]. \tag{56}$$

The elliptic undeformed canopy shape chosen here is inspired by [Lennon and Pellegrino 2005], and is such that the deformed shape turns out to be quite similar to the oval shape obtained in the analysis of [Taylor 1919], but without the lobes (see discussion in Section 1). Moreover, in Taylor's optimal parachute the ratio of minimum to maximum diameter is about 0.6, and this is also the ratio obtained in our case. The parabolic shape was chosen not due to physical reasons but simply because this was the family of shapes considered in our previous investigation (see [Libai and Givoli 2002]).

We assume uniformly distributed pressure, except in one case discussed at the end of this section.

We use nondimensional parameter values which were chosen based on the following normalization. Denoting dimensional quantities with a *, we first define two reference quantities: the length L^*, related to the height Z of the undeformed membrane, and the force $F^* = E^*h^*L^*$. Due to technical reasons that we omit here, we define $L^* = Z/2$ for the parabolic canopy and $L^* = Z/3$ for the elliptic canopy, although of course the choice $L^* = Z$ would have been equally legitimate. Then all the parameters and variables are normalized, according to their units, with respect to a product of powers of L^* and F^*. Thus, for example, $p = p^*/(E^*h)$ and $T = T^*/(E^*h^*)$. This normalization method always gives the nondimensional quantity $Eh = 1$. All parameters that appear in the examples below are unitless, having been defined by using this method of normalization. In all the examples shown here we use the Hookean material law, and $\nu = 0.5$.

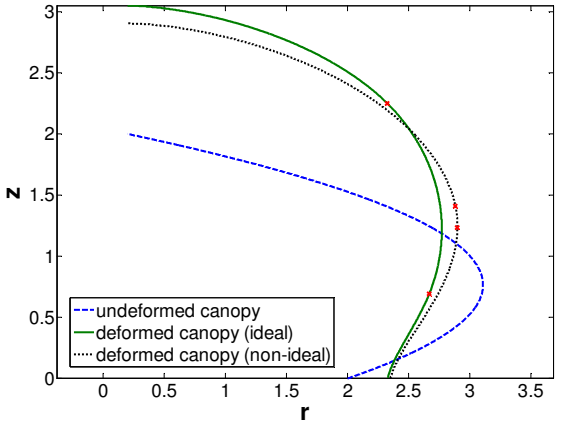

Figure 6. Undeformed and deformed shapes of a parabolic canopy with a central hole, under the applied load $P = 0.4$.

The computational tolerances needed for the double iteration loop are set as follows. In the case of a canopy with a central hole we use the tolerances $\delta_1 = 0.01$ and $\delta_2 = 10^{-3}$, while in the case of a canopy without a central hole we use $\epsilon_\phi = 0.07$, $\epsilon_1 = 10^{-4}$, and $\epsilon_2 = 5 \cdot 10^{-3}$. In all cases we take 10,000 steps in the z direction. This choice is based on practical convergence analysis; see [Ofir 2009] for the details and a convergence graph.

Figure 6 shows the undeformed and deformed shapes of the parabolic canopy with a central hole, under the load $P = 0.4$. The deformed shapes of both an ideal membrane and a nearly ideal membrane with $N_{\text{cr}} = -0.05$ are shown. Here and in subsequent figures, the boundaries of the wrinkle zone are marked on the deformed meridian by two $\times$ marks. It is clear that the wrinkle zone is much larger in the ideal membrane, as it should be. We also see that the deformed membranes are almost flat at the upper edge, which is consistent with the discussion at the end of Section 2.2.

Figure 7 shows the size of the wrinkle zone, relative to the entire meridian length, as a function of the applied load P, for four values of N_{cr}. In the case of the ideal membrane ($N_{\text{cr}} = 0$), the wrinkle

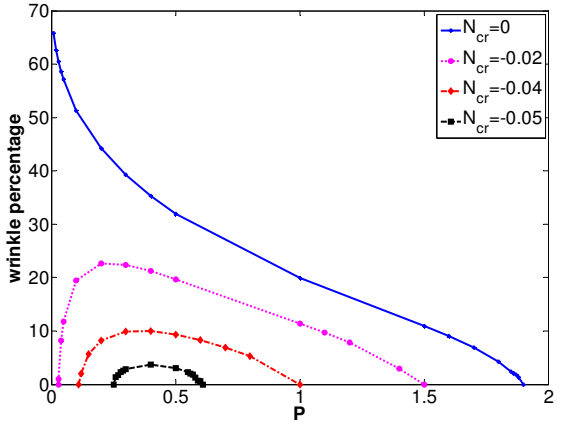

Figure 7. The wrinkle zone size as a function of the applied load P in a parabolic canopy with a central hole.

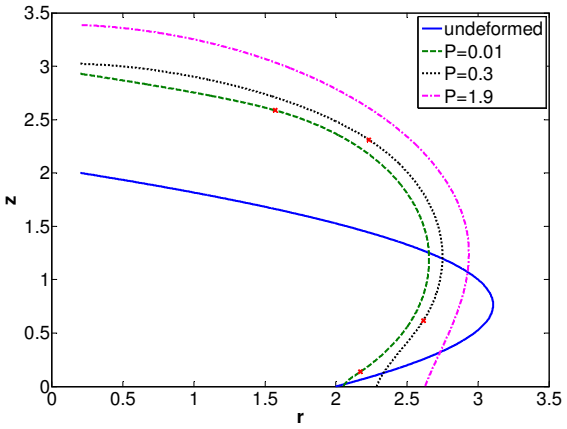

Figure 8. Response of a parabolic canopy with a central hole: undeformed and deformed shapes for three values of the vertical load P.

zone shrinks as P increases, up to a load value of about $P = 1.9$, beyond which the entire membrane becomes doubly tense. In the case of a nearly ideal membrane (that is, for *any* nonzero value of N_{cr}), the wrinkling behavior is considerably different. When the applied forces are very small, no wrinkles are present since the membrane has a certain capability of carrying compressional hoop stresses. When the applied loads are large enough, wrinkles start to form. Increasing the load further causes the wrinkle zone to expand, up to a maximal size. Increasing the load even further causes the wrinkle zone to shrink until it totally vanishes. The wrinkled regime shrinks when the value of $|N_{\mathrm{cr}}|$ is increased. The latter behavior is the more physical one, since real membranes are not ideal. Additional numerical examples in this context can be found in [Ofir 2009].

Figures 8 and 9 show the responses of the ideal parabolic canopy with a central hole, under an increasing applied load. In Figure 8 we show the undeformed and deformed shapes, and in Figure 9 the distribution of the stress resultants N_s and N_θ and the distribution of the stretches λ_s and λ_θ. Note that in the wrinkle zone $N_\theta \equiv 0$, and the hoop stretch λ_θ becomes nonphysical and is therefore not shown in this zone. For the three load values considered in these figures, the lowest one ($P = 0.01$) yields a very large wrinkle zone, the intermediate one ($P = 0.3$) gives a smaller wrinkle zone, and the highest one ($P = 1.9$) causes the membrane to be doubly tense along the entire meridian.

Figure 10 summarizes the response of a parabolic canopy with a central hole as a function of the applied load P. We show the maximal values along the meridian of the stress resultants N_s and N_θ and of the stretches λ_s and λ_θ. These functions are monotone but are far from being linear.

Figures 11 and 12 show the responses of a nearly ideal elliptic canopy with no central hole, under an increasing applied load. Here we set $N_{\mathrm{cr}} = -0.002$. Again we show the undeformed and deformed shapes (Figure 11), and the distributions of the stress resultants N_s and N_θ and of the stretches λ_s and λ_θ (Figure 12). In this case the response of the membrane is more sensitive to changes of the load value than in the previous case. Already for $P = 0.4$ the entire meridian is doubly tense.

Figure 13 shows the response of the ideal elliptic canopy with a central hole in two cases: one in which the pressure along the meridian is uniformly distributed, and the other in which it is distributed nonuniformly according to the function shown in Figure 4. We show the two deformed shapes in Figure 13a and the two meridional stress resultants in Figure 13b, for $P = 0.3$. The difference between the two

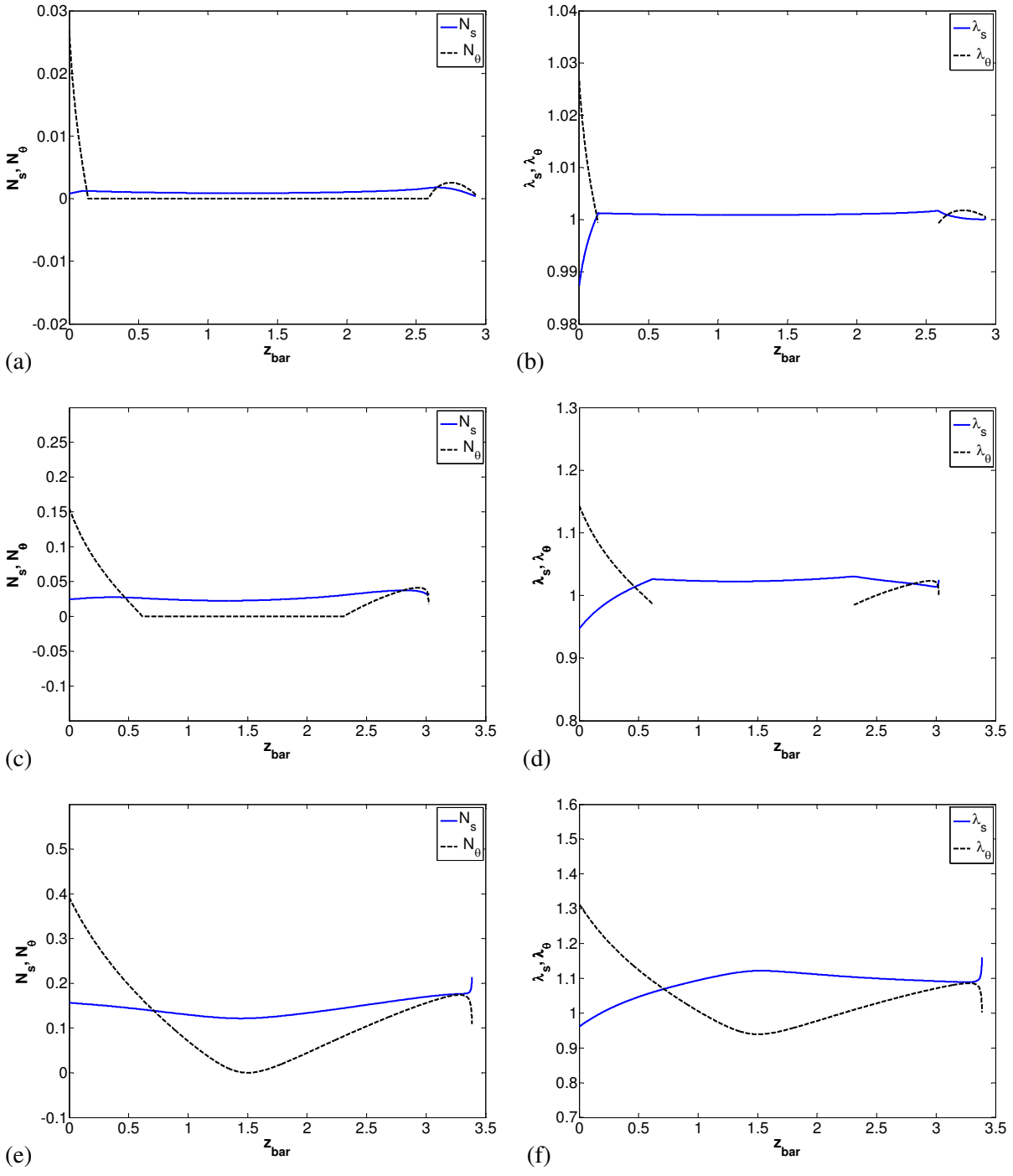

Figure 9. Response of a parabolic canopy with a central hole, stress resultant, and stretch distribution: (a) $P = 0.01$, stress resultants, (b) $P = 0.01$, stretches, (c) $P = 0.3$, stress resultants, (d) $P = 0.3$, stretches, (e) $P = 1.9$, stress resultants, (f) $P = 1.9$, stretches.

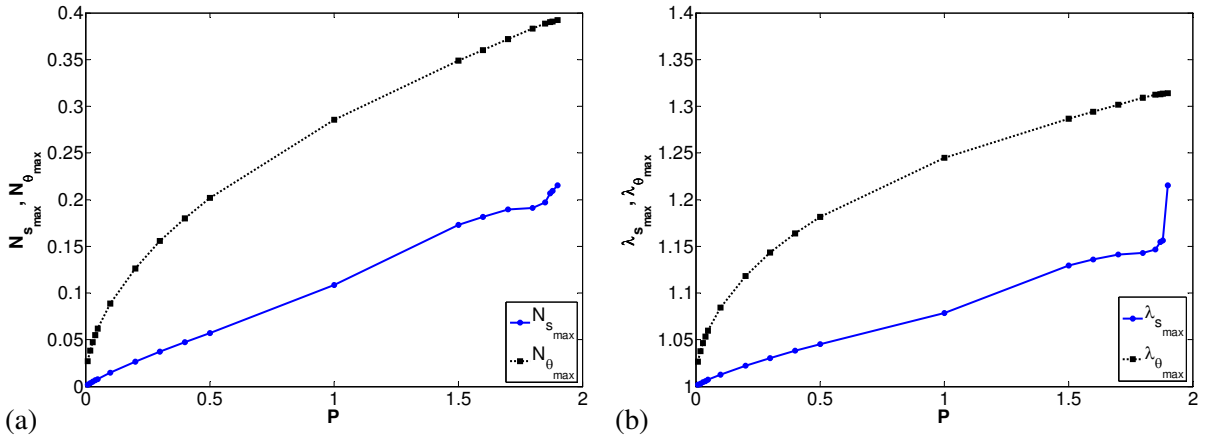

Figure 10. Response of a parabolic canopy with a central hole as a function of the applied load P: (a) maximal stress resultants, (b) maximal stretches.

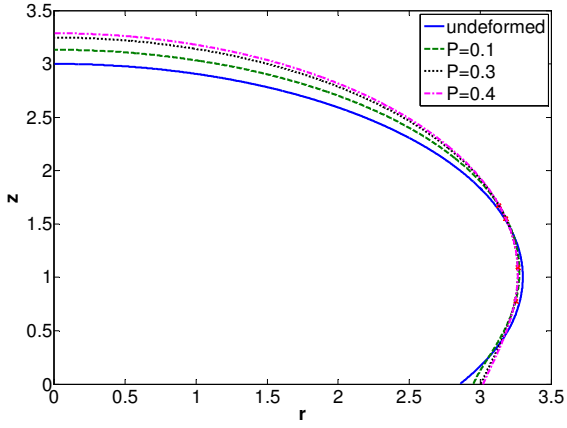

Figure 11. Response of a nearly ideal elliptic canopy with no central hole: undeformed and deformed shapes for three values of the vertical load P.

deformed shapes is small, although wrinkles are formed only in the case of uniform pressure distribution. However, the meridional stress in the vicinity of the hole is much larger in the case of uniform pressure. This shows that ignoring the effect of nonuniformity of pressure distribution on the mechanical response of the canopy is not always justified.

Finally we consider the case of an orthotropic canopy (see Section 4.1). We use an ideal membrane with the elliptic undeformed shape and a central hole, and with the vertical load $P = 0.3$. The nondimensional Young's modulus in the circumferential direction is still $E_\theta h = 1$, while in the meridional direction we take $E_s = 2E_\theta = 2$. The Poisson ratio is taken as 0.5 in both directions. In Figures 14a and 14b we compare the meridional stress resultant N_s and stretch λ_s, respectively, in the isotropic and orthotropic cases. We see that the orthotropy does not affect N_s along the meridian except near the hole surface, where the effect is very strong. The stretch λ_s is affected almost uniformly along the meridian. The deformation and circumferential stress and stretch (not shown here) are affected much less by the orthotropy.

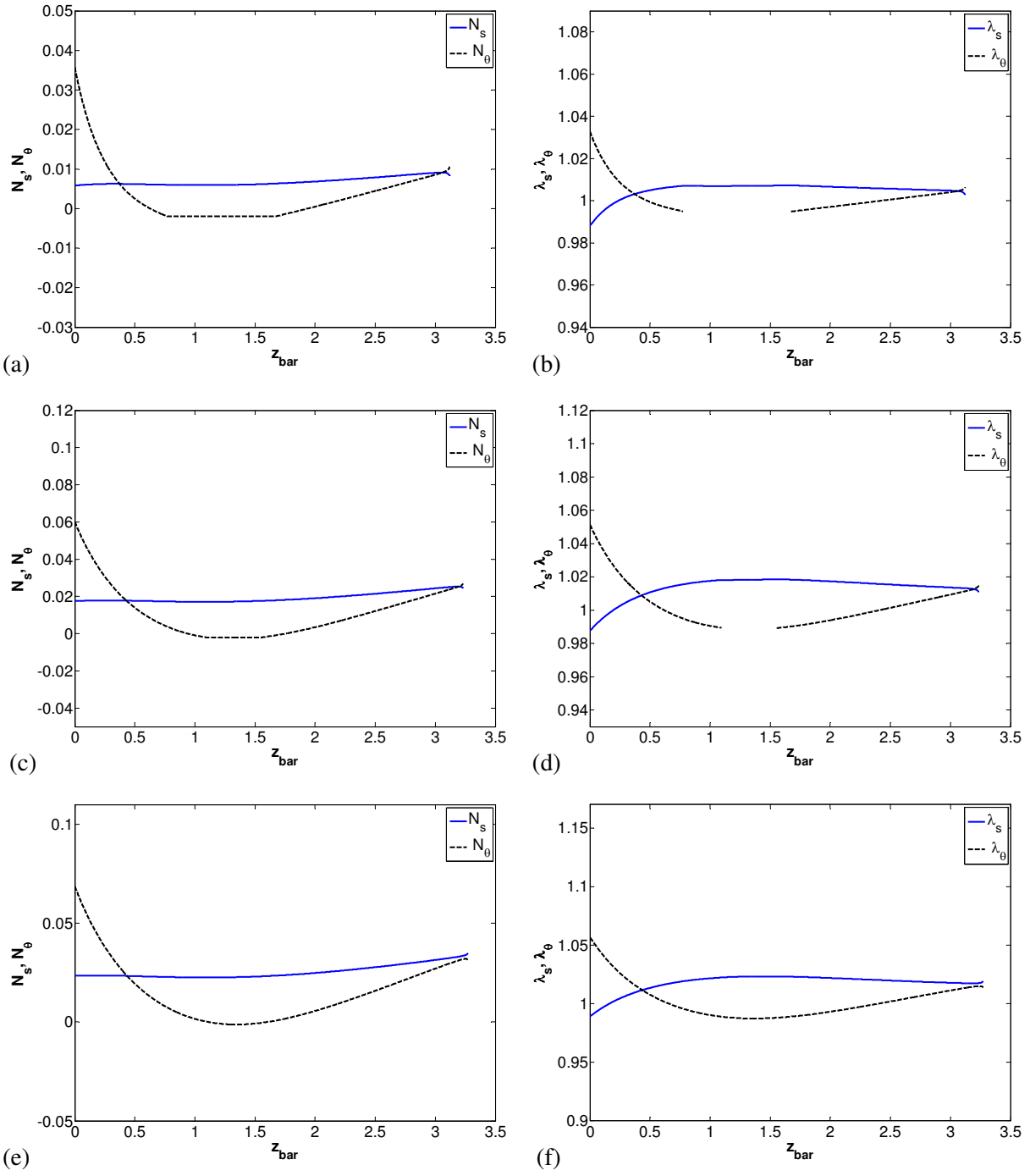

Figure 12. Response of a nearly ideal elliptic canopy with no central hole, stress resultants, and stretch distribution: (a) $P = 0.1$, stress resultants, (b) $P = 0.1$, stretches, (c) $P = 0.3$, stress resultants, (d) $P = 0.3$, stretches, (e) $P = 0.4$, stress resultants, (f) $P = 0.4$, stretches.

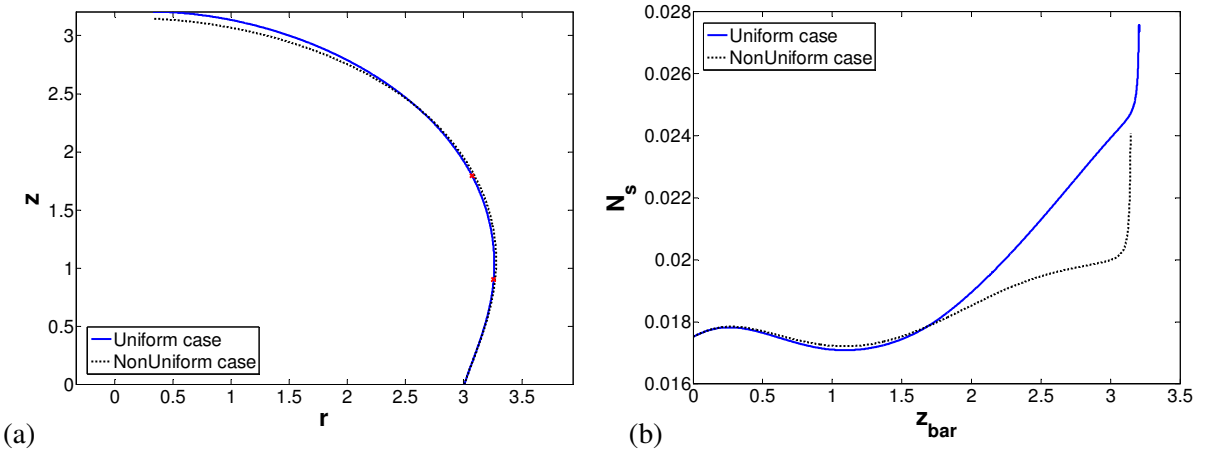

Figure 13. An ideal elliptic canopy with a central hole — responses in the cases of *uniformly and nonuniformly distributed pressure*: (a) deformed shapes, (b) meridional stress resultant.

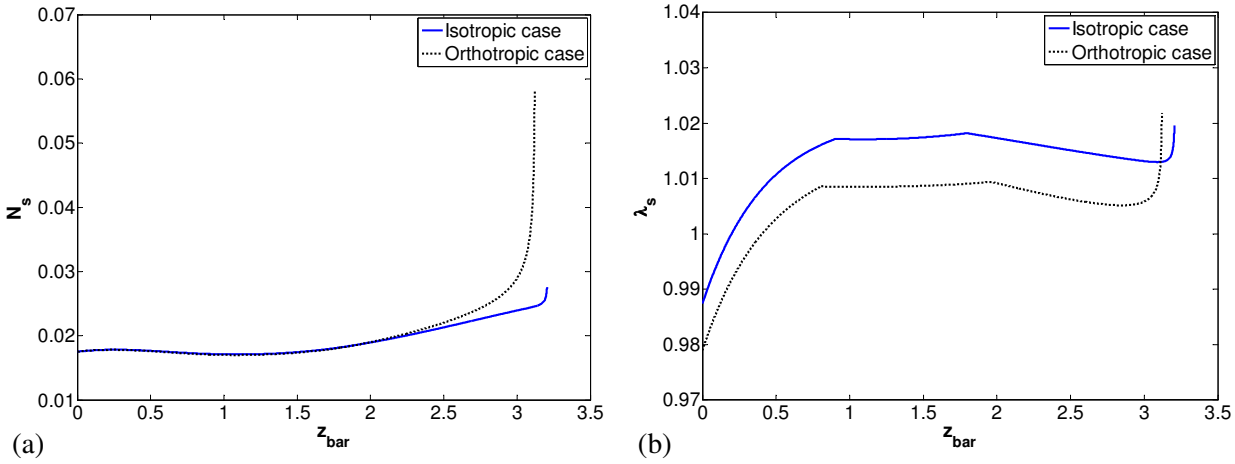

Figure 14. Comparison between the responses of isotropic and orthotropic canopies: (a) meridional stress resultant N_s, (b) meridional stretch λ_s.

6. Concluding remarks

The problem considered in this paper, of the quasistatic behavior of parachute canopies including the effects of large deformation and wrinkling, belongs to an important class of problems in nonlinear membrane shell theory. Other examples of such problems can be found, for example, in biology. In the present paper we have extended [Libai and Givoli 2002], which used wrinkle fields (also called tension fields) to model the wrinkle zones, but considered a much simplified setup.

The model introduced here, which represents a parachute under axisymmetric geometry, material properties, and loading, was analyzed via a double-iteration numerical procedure, based on a shooting technique and incremental loading. We first considered a canopy with a small central hole, made of an

isotropic Hookean material, and we assumed uniform pressure distribution. Later we showed how to relax these assumptions.

The advantage of the proposed numerical scheme employed here, over, say, the finite element method (FEM), is that it is quite simple, very easy to implement, and exhibits fast convergence, despite the complexity of the problem which involves the highly nonlinear membrane shell equations, different regions with interfaces which are unknown a priori, and deformation-dependent pressure magnitude. An attack of the same class of axisymmetric problems by FEM would be much more complicated. However, our method is restricted by the strong assumption of axial symmetry. It may be possible to extend it for more realistic nonaxisymmetric scenarios by using Fourier decomposition and considering the modal response to sinusoidal loading (see, for example, [Givoli and Libai 1995]). However, it may well be the case that for such problems one should resort to FEM.

Acknowledgments. This work was partly supported by the Fund for the Promotion of Research at the Technion and the fund provided through the Lawrence and Marie Feldman Chair in Engineering. The authors are grateful to the two anonymous reviewers for their very helpful comments.

References

[Baginski et al. 2006] F. Baginski, K. A. Brakke, and W. W. Schur, "Stability of cyclically symmetric strained pumpkin balloons and the formation of undesired equilibria", *J. Aircr.* **43**:5 (2006), 1414–1423.

[Cavicchi et al. 2009] A. Cavicchi, L. Gambarotta, and R. Massabò, "Computational modeling of reconstructive surgery: the effects of the natural tension on skin wrinkling", *Finite Elem. Anal. Des.* **45**:8-9 (2009), 519–529.

[Chiu et al. 1993] H. C. Chiu, R. C. Benson, M. D. Fiscella, and S. J. Burns, "Mechanical and thermal wrinkling of polymer membranes", pp. 1–4 in *Proc. 1993 ASME Winter Annual Meeting* (New Orleans, LA), ASME, New YorK, 1993.

[Deng and Pellegrino 2008] X. Deng and S. Pellegrino, "Computation of partially inflated shapes of stratospheric balloon structures", in *Proc. 49th AIAA/ASME/ASCE/AHS/ASC Structures, Structural Dynamics, and Materials Conference* (Schaumburg, IL), 2008. paper AIAA-2008-2133.

[Givoli and Libai 1995] D. Givoli and A. Libai, "Incremental stresses in loaded orthotropic circular membrane tubes, II: numerical solution", *Int. J. Solids Struct.* **32**:13 (1995), 1927–1947.

[Irvine and Montauban 1980] H. M. Irvine and P. H. Montauban, "On hot air balloons", *Int. J. Mech. Sci.* **22**:10 (1980), 637–649.

[Jeong and Kwak 1992] D. G. Jeong and B. M. Kwak, "Complementarity problem formulation for the wrinkled membrane and numerical implementation", *Finite Elem. Anal. Des.* **12**:2 (1992), 91–104.

[Kim and Peskin 2006] Y. Kim and C. S. Peskin, "2-D parachute simulation by the immersed boundary method", *SIAM J. Sci. Comp.* **28**:6 (2006), 2294–2312.

[Kim and Peskin 2009] Y. Kim and C. S. Peskin, "3-D parachute simulation by the immersed boundary method", *Comput. Fluids* **38**:6 (2009), 1080–1090.

[Lennon and Pellegrino 2005] A. Lennon and S. Pellegrino, "Structural mechanics of lobed inflatable structures", pp. 1–12 in *Proc. European Conf. on Spacecraft Structures, Materials & Mechanical Testing* (Noordwijk, The Netherlands), European Space Agency, Noordwijk, The Netherlands, 2005. ESA SP-581.

[Li and Steigmann 1995a] X. Li and D. J. Steigmann, "Finite deformation of a pressurized toroidal membrane", *Int. J. Non-Linear Mech.* **30**:4 (1995), 583–595.

[Li and Steigmann 1995b] X. Li and D. J. Steigmann, "Point loads on a hemispherical elastic membrane", *Int. J. Non-Linear Mech.* **30**:4 (1995), 569–581.

[Libai 1990] A. Libai, "The transition zone near wrinkles in pulled spherical membranes", *Int. J. Solids Struct.* **26**:8 (1990), 927–939.

[Libai and Givoli 2002] A. Libai and D. Givoli, "Analysis of pulled axisymmetric membranes with wrinkling", *Int. J. Solids Struct.* **39**:5 (2002), 1259–1274.

[Libai and Simmonds 1998] A. Libai and J. G. Simmonds, *The nonlinear theory of elastic shells*, Cambridge University Press, 1998.

[Liu and Sze 2009] X. H. Liu and K. Y. Sze, "A corotational interpolatory model for fabric drape simulation", *Int. J. Numer. Methods Eng.* **77**:6 (2009), 799–823.

[Liu et al. 2001] X. Liu, C. H. Jenkins, and W. W. Schur, "Large deflection analysis of pneumatic envelopes using a penalty parameter modified material model", *Finite Elem. Anal. Des.* **37**:3 (2001), 233–251.

[Lu et al. 2001] K. Lu, M. Accorsi, and J. Leonard, "Finite element analysis of membrane wrinkling", *Int. J. Numer. Methods Eng.* **50**:5 (2001), 1017–1038.

[Mosler and Cirak 2009] J. Mosler and F. Cirak, "A variational formulation for finite deformation wrinkling analysis of inelastic membranes", *Comput. Methods Appl. Mech. Eng.* **198**:27-29 (2009), 2087–2098.

[Muttin 1996] F. Muttin, "A finite element for wrinkled curved elastic membranes, and its application to sails", *Commun. Numer. Methods Eng.* **12**:11 (1996), 775–785.

[Ofir 2009] Y. Ofir, "Analysis of stresses and wrinkles in a parachute canopy model using "wrinkle fields"", M.Sc. thesis, Dept. of Aerospace Engineering, Technion, Haifa, Israel, 2009, Available at http://www.graduate.technion.ac.il/Theses/Abstracts.asp?Id=24297.

[Pipkin 1986] A. C. Pipkin, "The relaxed energy density for isotropic elastic membranes", *IMA J. Appl. Math.* **36**:1 (1986), 85–99.

[Raible et al. 2005] T. Raible, K. Tegeler, S. Löhnert, and P. Wriggers, "Development of a wrinkling algorithm for orthotropic membrane materials", *Comput. Methods Appl. Mech. Eng.* **194**:21-24 (2005), 2550–2568.

[Rimrott and Cvercko 1986] F. P. J. Rimrott and M. Cvercko, "Wrinkling in thin plates due to inplane body forces", pp. 19–48 in *Inelastic behaviour of plates and shells: IUTAM symposium* (Rio de Janeiro, 1985), edited by L. Bevilacqua et al., Springer-Verlag, Berlin, 1986.

[Roddeman et al. 1987a] D. G. Roddeman, J. Drukker, C. W. J. Oomens, and J. D. Janssen, "The wrinkling of thin membranes, I: theory", *J. Appl. Mech.* (*ASME*) **54**:4 (1987), 884–887.

[Roddeman et al. 1987b] D. G. Roddeman, J. Drukker, C. W. J. Oomens, and J. D. Janssen, "The wrinkling of thin membranes, II: numerical analysis", *J. Appl. Mech.* (*ASME*) **54**:4 (1987), 888–892.

[Sahu et al. 1995] J. Sahu, G. Cooper, and R. Benney, "3D parachute descent analysis using coupled CFD and structural codes", *AIAA paper* (1995), 269–277. A95-1580-CP.

[Shannon 2001] M. P. Shannon, "Experimental analysis of the pressure distribution on a 35-foot personal parachute", *AIAA paper* (2001), 114–121. A01-29265.

[Steigmann 1990] D. J. Steigmann, "Tension-field theory", *Proc. R. Soc. Lond. A* **429**:1876 (1990), 141–173.

[Steigmann and Pipkin 1989] D. J. Steigmann and A. C. Pipkin, "Axisymmetric tension fields", *Z. Angew. Math. Phys.* **40**:4 (1989), 526–542.

[Stein et al. 2000] K. R. Stein, R. J. Benney, V. Kalro, T. E. Tezduyar, J. W. Leonard, and M. Accorsi, "Parachute fluid-structure interactions: 3-D computation", *Comput. Methods Appl. Mech. Eng.* **190**:3-4 (2000), 373–386.

[Stein et al. 2001] K. R. Stein, R. J. Benney, T. E. Tezduyar, J. W. Leonard, and M. Accorsi, "Fluid-structure interactions of a round parachute: modeling and simulation techniques", *J. Aircr.* **38**:5 (2001), 800–808.

[Tait and Connor 1997] R. J. Tait and P. Connor, "On the expansion of a deformed cylindrical elastic membrane", *IMA J. Appl. Math.* **59**:3 (1997), 231–243.

[Tait et al. 1996] R. J. Tait, D. J. Steigmann, and J. L. Zhong, "Finite twist and extension of a cylindrical elastic membrane", *Acta Mech.* **117**:1-4 (1996), 129–143.

[Taylor 1919] G. I. Taylor, "On the shapes of parachutes", technical report written for the U.K. Advisory Committee for Aeronautics, 1919. Reprinted as pp. 26–37 in *The scientific papers of sir Geoffrey Ingram Taylor*, vol. **3**, edited by G. K. Batchelor, Cambridge University Press, Cambridge, 1958.

[Wong and Pellegrino 2006] Y. W. Wong and S. Pellegrino, "Wrinkled membranes, II: analytical models", *J. Mech. Mater. Struct.* **1**:1 (2006), 27–61.

[Wu 1978] C. H. Wu, "Nonlinear wrinkling of nonlinear membranes of revolution", *J. Appl. Mech.* (*ASME*) **45** (1978), 533–538.

[Zak 1982] M. Zak, "Statics of wrinkling films", *J. Elasticity* **12**:1 (1982), 51–63.

Received 12 Mar 2010. Revised 8 Sep 2010. Accepted 13 Sep 2010.

YOAV OFIR: joav.ofir@gmail.com
Department of Aerospace Engineering, Technion – Israel Institute of Technology, Haifa 32000, Israel

DAN GIVOLI: givolid@aerodyne.technion.ac.il
Department of Aerospace Engineering, Technion – Israel Institute of Technology, Haifa 32000, Israel

AVINOAM LIBAI: aer7501@technion.ac.il
Department of Aerospace Engineering, Technion – Israel Institute of Technology, Haifa 32000, Israel